Atomic Spectroscopy

Article

Simultaneous in-situ determination of major, trace elements and $Fe^{3+}/\sum Fe$ in spinel using EPMA

Lihui Jia,[a] Yi Chen,[a,b,*] Qian Mao,[a] Di Zhang,[a] Jiangyan Yuan,[a] Xiaoguang Li,[a] Shitou Wu,[a] and Danping Zhang[a]

[a] State Key Laboratory of Lithospheric Evolution, Institute of Geology and Geophysics, Chinese Academy of Sciences, Beijing 100029, P.R. China

[b] University of Chinese Academy of Sciences, Beijing 100049, P.R. China

Received: *October 21, 2021;* ***Revised:*** *January 26, 2022;* ***Accepted:*** *January 26, 2022;* ***Available online:*** *January 29, 2022.*

DOI: 10.46770/AS.2022.002

ABSTRACT: Spinel, an important mineral in basalts and ultramafic rocks on Earth, Mars, and the Moon, is sensitive to petrologic and geochemical processes, and redox evolution. Due to the small grain size of extraterrestrial samples, investigations on the composition of spinel samples including presence of trace elements and ferric iron have been hindered by the lack of appropriate in-situ analytical techniques with high spatial resolution and the shortage of reference materials. This paper presents a combined method of simultaneously measuring the major and trace elements, and $Fe^{3+}/\sum Fe$ ratio in spinel samples using electron probe microanalysis (EPMA). Our new EPMA method is performed under double beam condition at a beam current of 200 nA for trace elements (Ti, V, Mn, Co, Ni, and Zn) and 60 nA for major elements (Mg, Fe, Al, and Cr) with an acceleration voltage of 25 kV. In addition, large analyzing crystals and peak overlap corrections were applied to reduce the detection limits and improve the analytical precision. The detection limits of 16–55 μg/g (3σ) for trace elements were achieved, and the estimated accuracies for the major elements and trace elements were within ± 2 and ± 6% (1σ), respectively. We selected seven spinel samples from the Luobusha and Stillwater intrusions to evaluate the validity of our method. They were sufficiently homogeneous with a relative standard deviation (RSD) of ± 2.0% (1σ) for the major elements (except MgO in 16SW3-9) and ± 7.0% (1σ) for the trace elements. The EPMA results obtained for the major and trace elements of the most homogeneous spinel LBS13-04 were compared with those measured using X-ray fluorescence and laser ablation inductively coupled plasma mass spectrometry. These values were in good agreement with the uncertainty of the methods. Thus, this spinel is highly suitable as a reference material for in situ microanalysis. The $Fe^{3+}/\Sigma Fe$ ratios of high Cr# (57.7-79.1) spinel standards determined using Mössbauer spectroscopy varied from 0.07 to 0.27, which were used for secondary standard calibration method to determine the spinel $Fe^{3+}/\Sigma Fe$ ratio with an accuracy of < ± 0.04 (2σ). Our results offer a high-precision EPMA method that can simultaneously determine the major and trace elements together with the $Fe^{3+}/\Sigma Fe$ ratio in spinel. This method provides robust and precise data on spinel for small, precious, and rare terrestrial or extraterrestrial samples, which can be used to understand the formation and evolution of rocky planets.

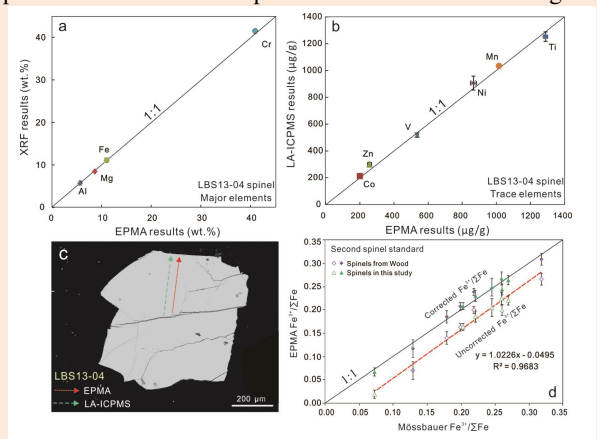

INTRODUCTION

Spinel ($(Mg, Fe^{+2})(Cr, Al, Fe^{+3})_2O_4$) is ubiquitous as a highly refractory accessory mineral that is regarded as an important petrologic and geochemical indicator.[1-4] The major elements (Mg, Fe, Cr, and Al) in spinel have been employed to discriminate tectonic settings[2,5] and assess mantle melting condition.[3,6,7] The variable proportions of several trace elements (*e.g.*, Sc, Ti, V, Mn, Co, Ni, and Zn) can provide information on the composition of magma and explore the mechanism responsible for their chemical variability.[8-10] Multi-valent elements in spinel (*e.g.*, Fe, Cr, and V) are highly sensitive to the redox state, which provides insight into the upper mantle and related mantle-derived magma oxygen fugacity (fO_2).[11,12] Therefore, studies on spinel have been a hot

topic in geoscience research over several decades.[5,13-16]

Recently, the sample capsule of Chang'E-5 successfully landed in Inner Mongolia, China, which has pushed the study of planetary science to a new high after Apollo.[17] Spinel is common in Lunar and Mars basalts and is closely associated with its meteoritic equivalents. Its structure and composition are uniquely responsive to changing temperature and oxygen fugacity.[1,3,7,18-21] Specifically, planetary basalts may be found in a reduced (IW-3), oxidized (Earth at FMQ), or intermediate (Mars) redox state.[21-26] Taking an expansive view, the spinel approach holds enormous promise toward understanding the magmatic differentiation of asteroids.[19,22,26] However, these significant application prospects have been hindered by the lack of suitable analytical techniques.

Laser ablation-inductively coupled plasma-mass spectrometry (LA-ICPMS) is well established for the determination of the mass fractions for trace elements in spinel. It has lower detection limits than electron probe microanalysis (EPMA) and can analyze a more comprehensive range of elements. However, there are still inevitable disadvantages, such as relatively poor spatial resolution and beam damage, given that the analyzed materials are evaporated and therefore, unavailable for further examination. Spinels that occur as inclusions in mafic-ultramafic rocks are small and always exhibit chemical zoning due to elemental exchange with co-existing silicates,[27] melt/rock interactions,[28] or complex metasomatic processes.[15] These are difficult to analyze using LA-ICPMS due to its low spatial resolution. In regard the analysis of the oxidation state of iron, several in-situ methods have been developed to determine the $Fe^{3+}/\sum Fe$ ratio in silicate minerals, such as Mössbauer spectroscopy,[29-31] X-ray absorption near-edge structure (XANES)[32-34] and energy-loss near-edge structure spectroscopy (ELNES),[35,36] which can provide non-destructive and moderate spatial resolution micro-analytical determination. However, the lack of spectral standards, high cost of analysis, and operational complexity make these methods unsuitable for small, precious, and rare extraterrestrial samples.

Recently, EPMA has become the backbone of numerous geochemical studies due to its unique characteristics, including high resolution, low cost, and non-destructive applicability.[37-39] For instance, Fialin *et al.*[40] established an empirical method to obtain the $Fe^{3+}/\sum Fe$ ratio for glasses. Höfer and Brey[41] developed a method to determine the major elements and Fe species in garnet using EPMA. To determine trace elements using EPMA, Su *et al.*[38] developed a method to investigate trace elements in olivine as sensitive tracers of mantle processes. The determination of the $Fe^{3+}/\sum Fe$ ratio or trace elements in spinel using EPMA has rarely been studied. Three gordian knots remain: 1) The shortage of spinel standards with known $Fe^{3+}/\sum Fe$ ratios, 2) the shortage of spinel standards for trace element analysis, and 3) the difficulties in reducing detection limits of trace elements in spinel.

In this study, we have studied new spinel standard materials for major and trace element analysis using EPMA, LA-ICPMS, and XRF, and for $Fe^{3+}/\sum Fe$ ratios using Mössbauer spectroscopy. Our optimized EPMA method can effectively reduce detection limits for trace elements in spinel and improve the analytical precision. In addition, spinel $Fe^{3+}/\Sigma Fe$ ratio was also determined using secondary standard calibration according to Wood and Virgo[30] and compared to the results obtained using Mössbauer spectroscopy. This study not only reports spinel reference standards with well-characterized values, but also develops an in-situ method that can be used to simultaneously determine the major and trace elements as well as $Fe^{3+}/\Sigma Fe$ ratio in spinel, altogether uniquely using EPMA. This method provides more precise and efficient technical support for the composition of spinel samples, which can be successfully applied to reveal the origin and evolution of rocky planets.

SAMPLE DESCRIPTION AND PREPARATION

Luobusha spinel. The Luobusha ophiolite is located approximately 200 km east-southeast of Lhasa in Southern Tibet and situated in the Indus-Yarlung Zangbu suture zone. The northern edge of the Luobusha ophiolite is in fault contact with the Tertiary Luobusha Formation. To the south, Triassic flysch-type sedimentary rocks structurally overlie the ophiolite with a fault contact. The podiform chromitites mainly occur in harzburgite and dunite, where the studied samples were collected.

Stillwater spinel. The Stillwater complex is a steeply dipping sub-volcanic intrusion that crops out on the northwestern margin of the Wyoming Craton.[42] It intruded Archean metasedimentary rocks and was overlain by Paleozoic and Mesozoic sedimentary rocks.[43] Three rock series have been described from the bottom to the top of the complex, including the Basal series, Ultramafic series, and Banded series. The Stillwater complex hosts world-class reserves of platinum-group elements and 80% of the Cr resources in the United States. The main chromite seams are within the ultramafic series. Typical chromitites exhibit massive or nodular textures. The samples analyzed in this study were collected from the cyclic chromitite units in the peridotite zone of the ultramafic series.

Sample preparation. In order to find spinel suitable to be used as standard material, many spinel samples were investigated. More than 400 thin sections were polished for the 231 spinel-bearing rock samples. The spinel samples that appear to be homogenous and free of inclusions based on an optical inspection and scanning electron microscopy (SEM) analysis were then tested for compositional homogeneity using EPMA. During the selection process, 108 out of 231 spinel samples were excluded because of mineral exsolution detectable using reflected light microscopy, and 81 out of the remaining 123 samples were excluded because

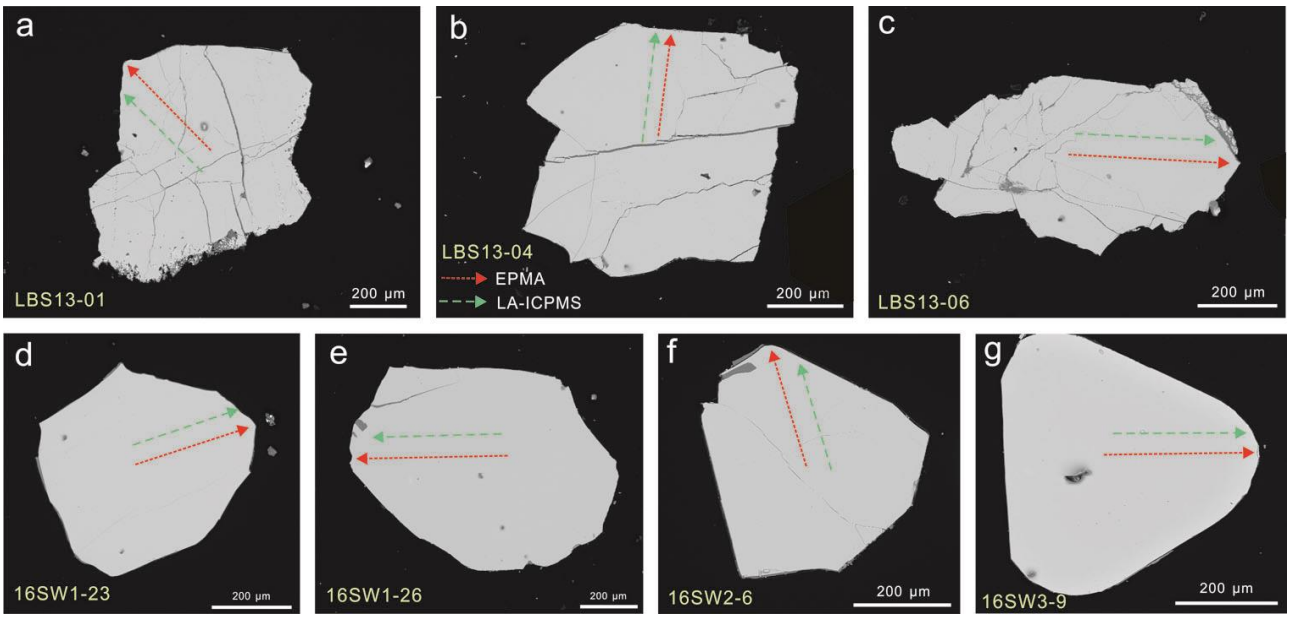

Fig. 1 Representative BSE images of the spinel samples from Luobusha ophiolite and Stillwater complex. a) LBS13-01, b) LBS13-04, c) LBS13-06, d) 16SW1-23, e) 16SW1-26, f) 16SW2-6, and g) 16SW3-9. The red lines show the sections of the EPMA analyzed spots and the green lines represent the LA-ICPMS analyzed spots.

of the chemical zoning visible in the backscatter electron (BSE) images. Only 42 spinel samples were qualified for our EPMA study. After the EPMA analysis, some of these spinel samples have heterogeneities and/or too low concentrations of the important trace elements. At last, only seven spinel samples were homogeneous in composition and designated as being suitable for use as reference material (Fig. 1). We selected spinel grains from each rock sample to prepare for the spinel epoxy mounts and pure spinel powders to finish the subsequent analysis.

ANALYTICAL TECHNIQUES

X-ray fluorescence (XRF) spectrometry. Major element data for whole-rock samples were obtained using XRF spectrometry on fused glass discs using a PANalytical AXIOS Minerals instrument at the Rock-Mineral Preparation and Analysis Laboratory at the Institute of Geology and Geophysics, Chinese Academy of Sciences (IGGCAS). The PANalytical AXIOS Minerals instrument was equipped with a Rh anode X-ray tube, which was set at an accelerating voltage of 40 kV. It is a sequential instrument with a single goniometer-based measuring channel covering the complete elemental measurement range from F to U in the concentration range from 1.0 μg/g to wt.% level, determined in vacuum media.[44] Glass discs for WD-XRF analysis were prepared upon the fusion of 0.6 g of the standard sample with 6.0 g of lithium tetraborate : metaborate (2:1) (Lithium borates 67-33, Claisse, Canada) using a Pt-Au crucible and mould employing electric fusion equipment (Claisse Fluxy, Corporation Scientific Claisse Inc., Quebec, Canada).[45] GSR-1, GSR-2, and GSR-3 were used to monitor the preparation process and instrument status.

Electron probe microanalysis (EPMA). The major and trace elements in the spinel samples were determined using a Cameca SXFive EPMA instrument equipped with a tungsten filament at the IGGCAS. The acceleration voltage was set to 25 kV and the beam currents for trace elements (Ti, V, Mn, Co, Ni, and Zn) and major elements (Cr, Al, Mg, and Fe) were 200 nA and 60 nA, respectively, with a beam diameter of 1 μm. The major and trace elements were acquired using five analyzing crystals as follows: Two TAP for Mg (Kα), Al (Kα), and Si (Kα), one LIF for Cr (Kα), Ni (Kα), and Mn (Kα), one LPET for Ti (Kα) and V (Kα), and one LLIF for Fe (Kα), Co (Kα), and Zn (Kα). Peak overlap corrections of Cr (Kß) to Mn (Kα) and Ti (Kß) to V (Kα) were applied. The natural minerals and synthetic oxides used for calibration were as follows: Rhodonite (Si and Mn), apatite (Ca), rutile (Ti), FeS_2 (Fe), ZnS (Zn), Cr_2O_3 (Cr), CoO (Co), NiO (Ni), MgO (Mg), and V_2O_5 (V). The peak counting times were 10 s for Al, Mg, and Fe; 20 s for Cr; 80 s for Ca, Ti, V, Co, and Zn; 120 s for Mn and Ni; and 240 s for P and Si. The background counting times were 5 s for Al, Mg, and Fe; 10 s for Cr; 40 s for Ca, Ti, V, Co, and Zn; 60 s for Mn and Ni; and 120 s for P and Si. A program based on the ZAF procedure was used for data correction (CITZAF).[46] The detection limits are 17 μg/g for Ti, 18 μg/g for V, 33 μg/g for Mn, 20 μg/g for Co, 55 μg/g for Ni, 48 μg/g for Zn, 16 μg/g for Ca, and 17 μg/g for Si, based on a 3σ estimate of the measured background variance.

Laser ablation inductively coupled plasma-mass spectrometry (LA-ICPMS). The trace elements in spinel were determined using

an Agilent 7500a quadrupole ICP-MS instrument (Agilent Technologies, USA) coupled with an Analyte G2 193 nm ArF excimer laser ablation system at the State Key Laboratory of Lithospheric Evolution, IGGCAS. The carrier gas, helium, was passed through the ablation cell, and argon was mixed downstream from the ablation cell. Prior to analysis, the pulse/analog (P/A) factor of the detector was calibrated using a standard tuning solution. The spot size and frequency of the laser were set to 44 μm and 5 Hz, respectively. The laser energy density was ~4.0 J/cm^2. All trace element determinations were carried out using time-resolved analysis in the fast, peak jumping mode. Each spot analysis consists of a ~20 s background and 60 s sample data acquisition. NIST SRM 610 reference glass was used as the calibration material, and ARM-1[47] and BCR-2G were analyzed for data quality control. Iron was used as an internal standard. The resulting data were reduced based on the GLITTER program.[48] For most trace elements (> 0.10 g/g), the accuracy is better than ± 10% with an analytical precision (1 RSD) of ± 10%. More details of the analytical procedures are provided in Xie *et al*.[49] and Wu *et al*.[50]

Mössbauer spectroscopy. Room-temperature ^{57}Fe Mössbauer spectra were recorded using a proportional counter and a Topologic 500A spectrometer at the Mössbauer Effect Data Center, Dalian Institute of Chemical Physics, Chinese Academy of Sciences. A ^{57}Co γ-ray radioactive source in rhodium was used, moving in constant acceleration mode within a velocity ramp of ± 10 mm/s. The velocity was calibrated relative to a 25 μm thick α-Fe foil using the positions certified for the (former) National Bureau of Standards standard reference material No. 1541; line widths of 0.28 mm/s (conventional source) and 0.36 mm/s (point source) for the outer lines of α-Fe were obtained at room temperature. Spectra were collected for 1–2 d and were fitted using the commercially available fitting program MössWinn. The relative content of the iron species was determined by integrating the absorption peak area of each phase.

RESULTS AND DISCUSSION

In general, the major and trace elements and $Fe^{3+}/\sum Fe$ ratio in spinel were determined using EPMA, LA-ICPMS, and Mössbauer spectroscopy, respectively. For the purpose of high spatial resolution, non-destructive, in-situ, and low-cost analysis, an EPMA method for the simultaneous determination of the major and trace elements together with $Fe^{3+}/\sum Fe$ ratio in spinel would be desirable, since this combination has rarely been studied to date. To achieve this, three steps are required: 1) Due to the shortage of suitable spinel trace element reference materials, the establishment of new spinel standards is critical for evaluating the precision of trace element analysis using EPMA; 2) the routine EPMA method yields high detection limits for trace elements (*e.g.*, V, Ti, Ni, Co, and Zn), typically two orders of magnitude higher than that using LA-ICPMS. The EPMA measurement procedure needs to be improved to achieve similar limits of detection; 3) the limited availability of spinel standards with known $Fe^{3+}/\sum Fe$ ratios have motivated research on more standard materials. Spinel $Fe^{3+}/\Sigma Fe$ ratios are commonly determined using charge imbalance based on EPMA data, which leads to large uncertainties in the $Fe^{3+}/\Sigma Fe$ ratios.[51] Wood and Virgo[30] reported a correction procedure to increase the accuracy of the $Fe^{3+}/\Sigma Fe$ ratio determination using EPMA. However, additional spinel standard samples with known $Fe^{3+}/\Sigma Fe$ ratios are desirable for the wide application of this method in geological samples.

High-precise determination of major and trace elements. The major and trace elements in spinel were measured using a Cameca SXFive EPMA at the IGGCAS. To achieve high precision and low detection limits, the optimal analytical conditions, including accelerating voltage, peak/background ratios, analytical crystals, beam currents, and peak overlap, were developed.

For the routine EPMA analysis of silicates and oxides, an accelerating voltage of 15 kV and a beam current of 20 nA are used in most laboratories with detection limits at a level of few tens or hundreds μg/g.[52,53] Increasing the accelerating voltage can lower detection limits, but may cause lower spatial resolution.[54] A higher accelerating voltage of 25 kV for both the major and trace element measurements was selected to reduce detection limits at good spatial resolution (1 μm) and to achieve higher count rates and better peak/background ratios. In addition, the beam current and count time can also contribute to reducing the detection limits. Using the CAMECA SXFive EPMA instrument, double beam current condition at a constant accelerating voltage can be used within one analytical session. In this study, a beam current of 60 nA and a short peak counting time of 10–20 s can meet the precision for major elements (Mg, Al, Cr, and Fe), and a higher beam current of 200 nA and much longer peak count time of 80–240 s were applied to achieve an acceptable detection limit approximately 10 μg/g. The background count time for each element was set to half the peak count time. The detection limits and precision levels can also be improved using appropriate diffraction crystals, such as large analyzing crystals (LLIF and LPET). Higher count rates and sensitivities can be achieved with these larger crystals when compared with "normal" crystals (LIF and PET).[55,56] Two large and three normal analyzing crystals were used as follows: Two TAP for Mg (Kα), Al (Kα), and Si (Kα); one LIF for Cr (Kα), Ni (Kα), and Mn (Kα); one LPET for Ti (Kα) and V (Kα); and one LLIF for Fe (Kα), Co (Kα), and Zn (Kα). Accurate peak positions and peak overlap corrections are crucial for achieving high analytical precision using EPMA. The peak overlap correction function in CAMECA software was used to eliminate interference, and the peak overlaps of Cr (Kß) with Mn (Kα) and Ti (Kß) with V (Kα) were corrected. A program based on the ZAF procedure was used for data correction (CITZAF).[46]

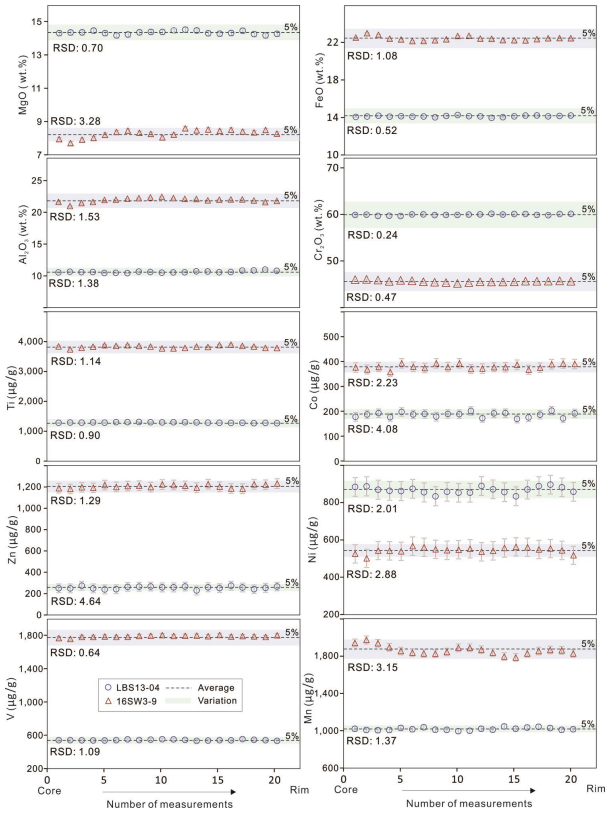

Fig. 2 The variations in the major and trace elements found in the spinel samples from LBS13-04 and 16SW3-9. Each point represents one analysis along the core-rim line. The shaded areas represent a variation of ± 5%. RSD: relative standard deviation.

In conclusion, the detection limits have been greatly improved as follows: 17 μg/g for Ti, 18 μg/g for V, 33 μg/g for Mn, 20 μg/g for Co, 55 μg/g for Ni, 48 μg/g for Zn, and 16 μg/g for Ca, based on a 3σ estimate of the measured background variance. Meanwhile, the estimated accuracies for the trace elements in spinel were within ± 12% (2σ), which were higher than those determined by routine EPMA method (20–30%, 2σ).

Homogeneity evaluation of the spinel references. The homogeneity of the major and trace elements is a fundamental requirement of any reference material.[37,57-59] A series of combined EPMA, XRF, and LA-ICP-MS investigations were carried out to evaluate the homogeneity of the spinel samples studied. All tables and Figs. 2 and 3 list the analytical results, including the mass fractions of the major and trace element, mean values, standard deviation of the mean (SD), and relative standard deviations (RSD), displaying the dispersion of the data.

LBS13-04 is the most homogeneous spinel among the seven selected Luobusha and Stillwater spinel samples. Fig. 2 shows the EPMA results obtained for this spinel together with spinel 16SW3-9 for comparison. The major elements, Mg, Fe, Al, and Cr, were homogeneous within ± 2% except for Mg in 16SW3-9 (± 3.3%, 1σ, Fig. 2). The trace elements, Ti, V, Ni, Co, Zn, and Mn, were also homogeneous within ± 5% (1σ) (Table 1). The trace elements were also determined using the LA-ICPMS technique, which is the best method for determining accurate mass fractions. Of the six trace elements determined using LA-ICPMS, Ti, Co, V, Ni, and Mn variations were homogeneous within ± 4%, while Zn variation was within ± 4.6% (1σ). The consistency of the data obtained using different analytical techniques is considered as a measure of the data quality. A comparison of all the mass fraction results obtained using different techniques is displayed in Fig. 3 for spinel LBS13-04. All the investigated elements determined by EPMA

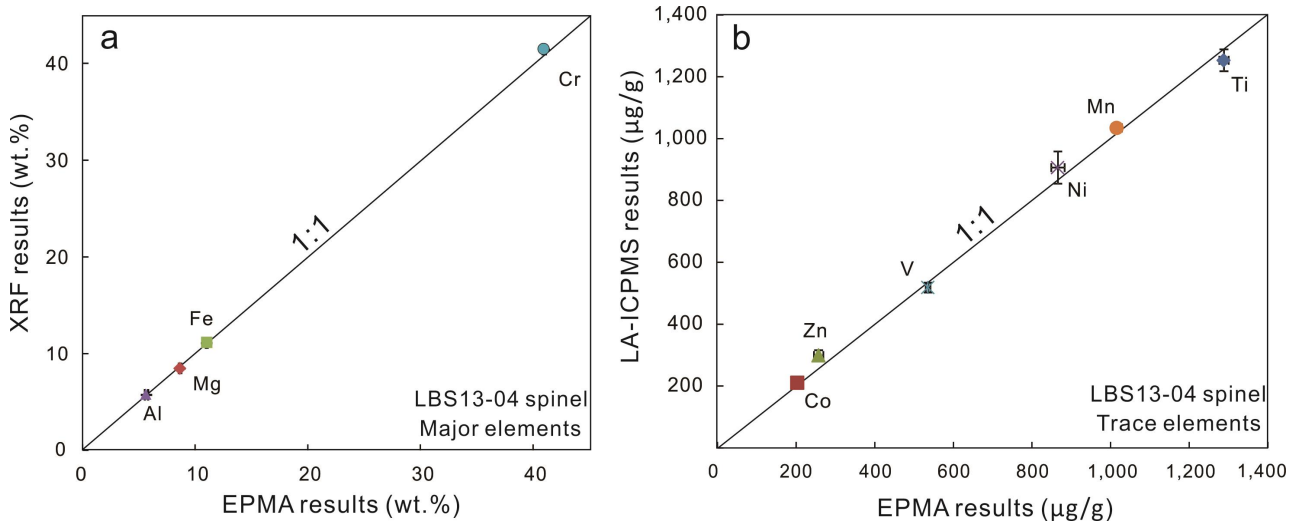

Fig. 3 A comparison of the major and trace element abundances in LBS13-04 determined using EPMA, LA-ICP-MS, and XRF. A 1:1 line is drawn in each plot for comparison purposes.

Table 1. The composition of the major and trace elements in the LBS13-04 spinel sample determined using EPMA, LA-ICPMS, and XRF

Method	Sample	Major elements (wt.%)				Trace elements (μg/g)					
		MgO	FeO	Al_2O_3	Cr_2O_3	Ti	Co	Zn	Ni	V	Mn
EPMA	LBS13-04-1	14.3	14.1	10.52	59.9	1282	191	251	883	540	1019
	LBS13-04-2	14.3	14.1	10.65	59.9	1291	198	251	886	539	1006
	LBS13-04-3	14.3	14.2	10.58	59.7	1285	202	275	868	538	1002
	LBS13-04-4	14.5	14.1	10.59	59.7	1293	190	250	862	537	1005
	LBS13-04-5	14.3	14.1	10.46	59.6	1286	207	241	861	536	1027
	LBS13-04-6	14.2	14.1	10.46	60.0	1302	198	242	873	540	1012
	LBS13-04-7	14.2	14.1	10.43	60.0	1300	200	264	853	549	1035
	LBS13-04-8	14.4	14.0	10.66	59.8	1308	191	267	833	543	1008
	LBS13-04-9	14.4	14.2	10.61	59.9	1299	200	267	857	547	1007
	LBS13-04-10	14.4	14.3	10.49	59.9	1296	199	260	853	551	994
	LBS13-04-11	14.5	14.1	10.54	60.0	1300	211	259	852	549	998
	LBS13-04-12	14.5	14.1	10.56	60.0	1299	186	268	888	543	1019
	LBS13-04-13	14.5	14.0	10.71	60.1	1294	202	230	870	531	1008
	LBS13-04-14	14.3	14.0	10.68	60.0	1285	203	261	855	536	1043
	LBS13-04-15	14.3	14.1	10.56	60.1	1281	184	253	834	540	1019
	LBS13-04-16	14.3	14.2	10.61	60.1	1276	189	276	869	538	1031
	LBS13-04-17	14.5	14.2	10.83	59.9	1279	198	258	886	552	1040
	LBS13-04-18	14.2	14.1	10.86	59.8	1268	211	242	895	545	1026
	LBS13-04-19	14.2	14.2	10.99	60.1	1275	185	256	881	539	1008
	LBS13-04-20	14.3	14.2	10.79	60.1	1267	202	267	857	532	1012
	Mean	14.3	14.1	10.6	59.9	1288	197	257	866	541	1016
	1σ	0.10	0.07	0.15	0.14	11.66	8.05	12.03	17.42	5.92	13.95
	RSD	0.70	0.52	1.38	0.24	0.90	4.08	4.68	2.01	1.09	1.37
LA-ICPMS	LBS13-04-1	14.8	11.0	8.22	63.6	1219	209	276	951	504	1020
	LBS13-04-2	14.8	11.0	8.06	61.9	1292	211	245	896	542	1033
	LBS13-04-3	15.1	11.0	8.24	61.9	1233	211	276	924	509	1033
	LBS13-04-4	13.5	11.0	7.43	55.3	1206	209	253	878	555	1047
	LBS13-04-5	14.8	11.0	8.11	60.8	1208	208	266	940	539	1024
	LBS13-04-6	14.8	11.0	8.15	60.3	1246	208	271	969	502	1044
	LBS13-04-7	14.9	11.0	8.14	60.6	1222	209	284	937	502	1033
	LBS13-04-8	14.6	11.0	8.04	60.0	1291	218	272	947	496	1034
	LBS13-04-9	14.6	11.0	7.92	59.3	1198	205	284	952	525	1018
	LBS13-04-10	15.2	11.0	8.27	61.8	1224	204	256	876	516	1038
	LBS13-04-11	15.0	11.0	8.16	61.4	1191	210	266	892	509	1046
	LBS13-04-12	15.1	11.0	8.25	61.5	1288	216	279	889	513	1042
	Mean	14.78	11.0	8.08	60.7	1235	210	269	921	518	1034
	1σ	0.44	0.00	0.23	2.03	36.56	3.98	12.49	32.76	18.53	9.88
	RSD	2.98	0.00	2.83	3.35	2.96	1.90	4.64	3.56	3.58	0.95
XRF	LBS13-04	14.2	14.3	10.8	60.9	1275	216	249	814	519	1042
	RE	1.15	-1.34	-1.71	-1.69	4.34	-5.92	-4.43	-5.98	4.54	-1.78

σ, standard deviation; RSD, relative standard deviation; RE, relative error.

and LA-ICPMS plot well along the 1:1 correspondence line with an RE < ± 5% (1σ) with the exception of Co and Ni (± 5.9 and ± 6.0%, respectively; Fig. 3a-b and Table 1). In addition, a comparison between the EPMA and XRF results indicates their

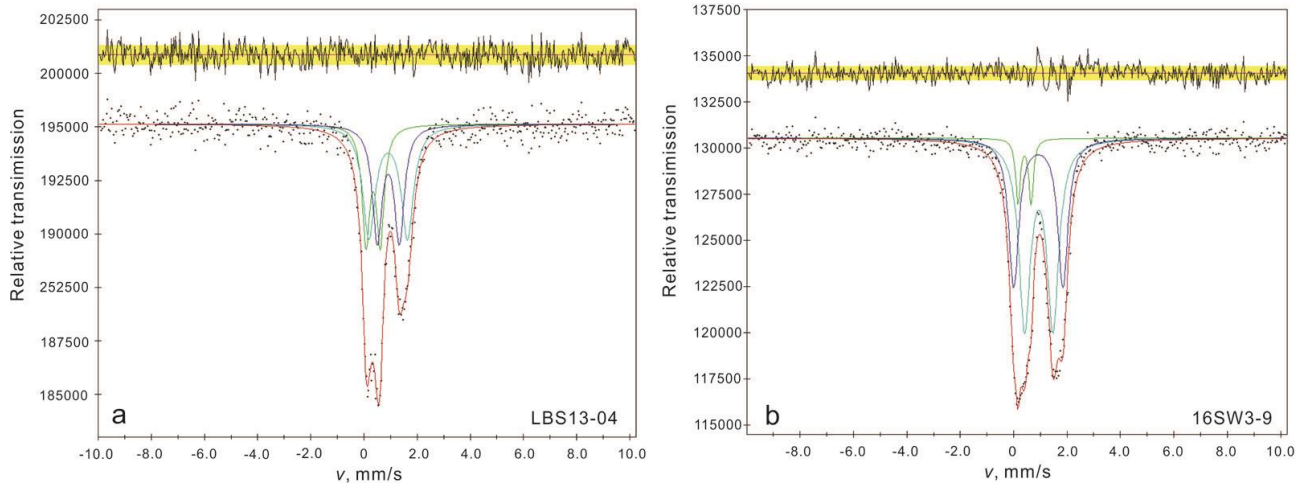

Fig. 4 Room-temperature ^{57}Fe Mössbauer spectroscopy of LBS13-04 and 16SW3-9 spinel samples.

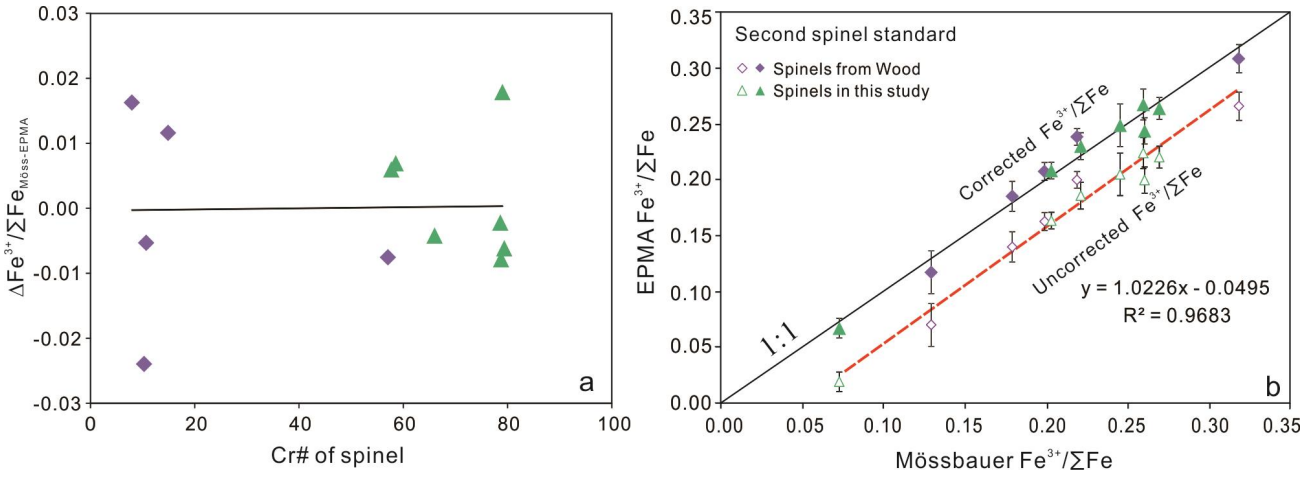

Fig. 5 (a) The relationship between Cr# and $\Delta Fe^{3+}/\Sigma Fe_{Möss\text{-}EPMA}$ in the uncorrected analyses of the spinel standards. Cr# and $\Delta Fe^{3+}/\Sigma_{FeMöss\text{-}EPMA}$ are uncorrelated ($R^2 = 0.0005$) and $\Delta Fe^{3+}/\Sigma Fe_{Möss\text{-}EPMA}$ was near zero. (b) A comparison of the spinel $Fe^{3+}/\Sigma Fe$ ratios measured using EPMA were well correlated with the ratios obtained using Mössbauer spectrometry, showing the reliability of the secondary standard calibration method.

outstanding agreement for the major elements investigated in this study (Fig. 3c-d). The relative errors did not exceed ± 2% (1σ) (Table 1). Therefore, LBS13-04 can be regarded as homogeneous for all the major and trace elements, and has the highest potential to be used as a reference material.

The homogeneity of the six other spinel samples was also tested using EPMA. In each spinel sample, 20 spots in a core-to-rim section were analyzed, yielding an RSD of only ± 2.0% (1σ) for the major elements (Fig. S1 and Fig. 2 for 16SW3-9) with the exception of MgO in spinel 16SW3-9 (RSD = ± 3.3%, 1σ), which emphasizes the high homogeneity of these spinel samples and the reproducibility of the measurements. The six trace elements determined in this study, all trace elements of 16SW1-23, 16SW1-26, 16SW2-6, and 16SW3-9 spinels were homogeneous within ± 5% (1σ) (Fig. S1). Ti, Mn, Co, V, and Ni in spinel LBS13-01 were in agreement by ± 4% (1σ), whereas Zn yields an RSD of ± 5.10% (1σ). The RSD values of LBS13-06 were ± 2.31%, ± 6.05%, ± 4.23%, ± 3.11%, ± 2.37%, and ± 2.13% (1σ) for Ti, Co, Zn, Ni, V, and Mn, respectively. We conclude that all the studied spinel samples can be regarded as homogeneous for all the major and trace elements.

Secondary standard calibration for the spinel $Fe^{3+}/\Sigma Fe$ ratio. Spinel $Fe^{3+}/\Sigma Fe$ ratios are commonly obtained by charge imbalance based on EPMA data, which may lead to large uncertainties in the $Fe^{3+}/\Sigma Fe$ ratios. Wood and Virgo[30] presented a correction procedure for spinel to increase the accuracy of the $Fe^{3+}/\Sigma Fe$ ratio determined using EPMA, which is based on the relationship between the difference in the $Fe^{3+}/\Sigma Fe$ ratio obtained using Mössbauer spectroscopy and EPMA ($\Delta Fe^{3+}/\Sigma Fe_{Möss\text{-}EPMA}$) and Cr# of the spinel standards. Subsequent studies have mainly

Table 2. Average composition of the major and trace elements and $Fe^{3+}/\sum Fe$ in the spinel samples determined using EPMA and Mössbauer spectroscopy

Comment	LBS13-01		LBS13-04		LBS13-06		16SW1-23		16SW1-26		16SW2-6	
Number of analyses	20		20		20		20		20		20	
	Mean	1σ	Mean	1σ	Mean	1σ	Mean	1σ	Mean	1σ	Mean	1σ
Major elements (wt.%)												
MgO	15.0	0.10	14.3	0.10	14.8	0.20	14.0	0.16	11.3	0.11	11.5	0.21
FeO	13.6	0.13	14.1	0.07	13.4	0.08	14.6	0.06	20.5	0.07	22.0	0.16
Al_2O_3	10.8	0.11	10.6	0.15	10.9	0.18	10.8	0.11	17.2	0.08	21.0	0.11
Cr_2O_3	60.2	0.13	59.9	0.14	60.1	0.23	59.8	0.14	49.8	0.14	44.4	0.13
Trace elements (μg/g)												
Ti	1370	18	1288	12	1319	31	1294	13	2869	24	2749	31
Co	209	8	197	8	185	11	205	10	195	7	232	6
Zn	274	14	257	12	254	11	266	9	442	12	532	10
Ni	836	29	866	17	962	30	829	39	827	21	930	16
Si	117	11	177	14	95	15	175	134	92	7	162	331
V	551	6	541	6	565	13	562	6	1303	7	1509	8
Mn	1044	27	1016	14	901	19	1058	19	1325	13	1492	19
Total*	100.3		99.6		99.9		99.8		99.9		100.0	
Cr#	78.89	0.18	79.09	0.22	78.68	0.33	78.83	0.20	66.05	0.13	58.58	0.16
$Fe^{3+}/\sum Fe_{EPMA\_uncorr}$	0.22	0.01	0.20	0.01	0.20	0.02	0.19	0.01	0.16	0.01	0.22	0.01
$Fe^{3+}/\sum Fe_{EPMA\_corr}$	0.27		0.24		0.25		0.23		0.21		0.26	
$Fe^{3+}/\sum Fe_{Möss}$	0.26		0.26		0.25		0.22		0.20		0.27	
$\triangle Fe^{3+}/\sum Fe_{MöSS\text{-}EPMA}$	-0.007		0.018		-0.002		-0.008		-0.004		0.007	
Comment	**16SW3-9**		**BAR8601****		**MHP79****		**IB8703****		**DB8803-3****		**KLB8320****	
Number of analyses	20		10		10		10		10		10	
	Mean	1σ	Mean	1σ	Mean	1σ	Mean	1σ	Mean	1σ	Mean	1σ
Major elements (wt.%)												
MgO	8.26	0.27	20.6	0.10	19.7	0.15	19.0	0.35	14.1	0.15	20.1	0.05
FeO	22.4	0.24	10.4	0.09	11.2	0.43	14.7	0.29	16.3	0.14	12.3	0.06
Al_2O_3	21.9	0.33	58.0	0.12	59.9	0.40	52.3	1.01	23.1	0.10	57.3	0.16
Cr_2O_3	45.6	0.22	10.3	0.06	7.72	0.44	13.0	0.92	45.7	0.07	9.71	0.05
Trace elements (μg/g)												
Ti	3826	44	1202	6	678	53	440	12	492	5	726	4
Co	372	8	156	10	200	26	240	8	220	6	200	4
Zn	1203	16	615	11	964	110	1353	13	903	15	891	12
Ni	545	16	2543	31	2606	262	2884	76	1096	17	2674	14
Si	142	74	1071	86	339	222	119	13	157	8	259	57
V	1787	11	470	5	416	34	535	11	1166	6	568	4
Mn	1860	59	639	14	666	68	840	23	1180	24	751	9
Total*	99.7		100.3		99.3		99.9		100.0		100.2	
Cr#	57.73	0.47	10.61	0.06	7.87	0.50	14.30	1.10	57.05	0.11	10.21	0.07
$Fe^{3+}/\sum Fe_{EPMA\_uncorr}$	0.02	0.01	0.14	0.01	0.07	0.02	0.27	0.01	0.16	0.01	0.20	0.01
$Fe^{3+}/\sum Fe_{EPMA\_corr}$	0.07		0.19		0.11		0.31		0.21		0.24	
$Fe^{3+}/\sum Fe_{Möss}$	0.07		0.18		0.13		0.32		0.20		0.22	
$\triangle Fe^{3+}/\sum Fe_{MöSS\text{-}EPMA}$	0.006		-0.005		0.016		0.012		-0.008		-0.020	

* Totals include the trace elements calculated as oxides.

** BAR8601, MHP79, IB8703, DB8803, and KLB8320 spinel samples are from Wood and Virgo.[30]

Fig. 6 A comparison of the spinel $Fe^{3+}/\Sigma Fe$ ratios measured using Mössbauer spectroscopy and the modified values of the secondary standard calibration, which show its reproducibility.

focused on the correction between $\Delta Fe^{3+}/\Sigma Fe_{Möss\text{-}EPMA}$ and Cr#, which is weak and absent, and confirmed that it can improve the accuracy of the spinel $Fe^{3+}/\Sigma Fe$ ratios determined using EPMA.[60-61] However, the Cr# values of most spinel standards from Wood and Virgo30 are low, varying from 7.9 to 57.7, which cannot match the $Fe^{3+}/\Sigma Fe$ ratio of high Cr# spinels. Therefore, the shortage of high Cr# spinel standards with known $Fe^{3+}/\Sigma Fe$ ratios is an insurmountable difficulty.

After testing the homogeneity of 42 Luobusha and Stillwater spinel samples using EPMA, we showed that seven spinel samples can be regarded as homogeneous for all the major and trace elements. When compared with previously reported spinel standards, the Cr# values of the studied spinel samples vary from 57.7 to 79.1. These spinels were analyzed using ^{57}Fe Mössbauer spectroscopy to ascertain spinel structure of the Fe-containing phase and to determine the $Fe^{3+}/\Sigma Fe$ ratio, as shown in Fig. 4 for LBS13-04 and 16SW3-9, and in Supplementary Fig. S2 for the other spinel samples. The $Fe^{3+}/\Sigma Fe$ ratios of LBS13-01, LBS13-04, and LBS13-06 were 0.261, 0.262, and 0.247, respectively. The $Fe^{3+}/\Sigma Fe$ ratios of the Stillwater spinel samples were 0.222, 0.204, 0.271, and 0.073 for 16SW1-23, 16SW1-26, 16SW2-6, and 16SW3-9, respectively (Table 2).

In this study, we investigated seven spinel standards and five additional spinel standard samples with known $Fe^{3+}/\Sigma Fe$ ratios from Wood and Virgo.[30] We tested 10–20 points on each sample using EPMA (Table S1). The spinel $Fe^{3+}/\Sigma Fe$ ratios were calculated from the EPMA measurements based on the perfect stoichiometry in the first step. The $\Delta Fe^{3+}/\Sigma Fe_{Möss\text{-}EPMA}$ and Cr# of these spinel standards were uncorrelated and the slope of the best-fit line was approximately zero (Fig. 5a). Therefore, we chose to apply a single linear correction to the spinel $Fe^{3+}/\Sigma Fe$ ratio, which did not vary with Cr# value. The results suggest that the average $Fe^{3+}/\Sigma Fe$ ratios calculated using EPMA, either of the spinel samples from Luobusha and Stillwater, or of the secondary spinel standards from Wood and Virgo,[30] were well correlated with the ratios obtained using Mössbauer spectrometry (Fig. 5b, uncorrected values). Using the data obtained for all of these spinel samples for calibration of the correction procedure (Table 2), a linear correction relationship was established. After correction, the spinel $Fe^{3+}/\Sigma Fe$ ratios obtained using EPMA were nearly identical to those obtained using Mössbauer spectroscopy, and the accuracy of the $Fe^{3+}/\Sigma Fe$ ratios was within ± 0.04 (2σ; Table 2).

In summary, the secondary standard calibration has been improved in regard two aspects in this study: 1) The systematic error of any element in the EPMA analysis can lead to an increase in the magnitude of $\Delta Fe^{3+}/\Sigma Fe_{Möss\text{-}EPMA}$.[30,60] The high-precision determination of the trace elements in spinel using EPMA (± 12%; 2σ) can effectively improve the systematic bias in the EPMA-derived $Fe^{3+}/\Sigma Fe$ ratio. 2) The precision of the corrected $Fe^{3+}/\Sigma Fe$ ratios decreases for samples that fall outside the compositional range of the correction standards used. The wider Cr# values ranging from 7.9 to 79.1 of the spinel standards could broaden the compositional range of the unknowns being analyzed. In addition, the error of two calibration curves established seven days apart was within ± 0.02 (Fig. 6 and Table S2), suggesting the stability of the EPMA measurements and the reproducibility of the secondary standard calibration method. Therefore, this method can be used to accurately correct the $Fe^{3+}/\Sigma Fe$ ratio of unknown spinel samples.

CONCLUSIONS

A new combined EPMA method for the simultaneous determination of the major and trace elements together with the $Fe^{3+}/\Sigma Fe$ ratio in spinel, has been developed using the CAMECA SXFive electron microprobe. A higher accelerating voltage of 25 kV, double beam current condition (60 nA for major elements and 200 nA for trace elements), large analyzing crystals, and peak overlap corrections were applied to reduce the detection limits and improve the analytical precision. The estimated accuracies for the major elements and trace elements were within ± 2 and ± 6% (1σ), respectively. For trace elements, detection limits in the range of 16–55 μg/g were achieved (3σ). Seven spinel samples from Luobusha and Stillwater were evaluated using EPMA and were sufficiently homogeneous to be used as secondary standards with RSDs within ± 2.0% (1σ) for the major elements and < ± 7.0% (1σ) for trace elements. In particular, LBS13-04 is the most homogeneous spinel sample in this set and well-characterized reference values were obtained for the major elements (Mg, Fe, Al, and Cr) and representative trace elements (Ti, Co, Zn, Ni, V, and Mn) were determined using EPMA, XRF, and LA-ICPMS methods. Thus, this spinel is highly suitable as a reference material for in-situ microanalysis. The $Fe^{3+}/\Sigma Fe$ ratios of the studied spinel

samples determined using Mössbauer spectroscopy vary from 0.07 to 0.27. High Cr# spinel standards were used as the secondary standard calibration method to determine the spinel $Fe^{3+}/\Sigma Fe$ ratio with an accuracy of $Fe^{3+}/\Sigma Fe$ ratio that is within ± 0.04 (2σ). In conclusion, seven spinel standards developed in this study may have important applications for new and informative interpretations of the origin and evolution of Earth, Lunar, Mars, and other planets.

ASSOCIATED CONTENT

The supporting information (Figs S1-S2; Tables S1-S2) is available at www.at-spectrosc.com/as/home

AUTHOR INFORMATION

Yi Chen is a research professor of geology at the Institute of Geology and Geophysics, Chinese Academy of Sciences (IGGCAS) in Beijing, China. He received his B.S. degree in Geology from China University of Geosciences (Wuhan) in 2003, and completed Ph.D. in petrology from the IGGCAS in 2008. He worked as a postdoctoral research fellow from 2008 to 2010 at the IGGCAS. His early research focused on thermodynamic modeling and high-grade metamorphism. His recent research interests have expanded to subduction zone crust-mantle interactions, subduction zone geodynamics, planetary materials, high-precision EPMA microanalyses and their applications to Earth and Planetary science. Currently, he is on the editorial board for Frontiers in Earth Science, and on the committee of Metamorphic Petrology in the Chinese Society for Mineralogy, Petrology and Geochemistry, and the committee of Petrology in Geological Society of China. He has published over 60 peer-reviewed scientific papers in ISI-indexed journals.

Corresponding Author

*Y. Chen

Email address: chenyi@mail.iggcas.ac.cn

Notes

The authors declare no competing financial interest.

ACKNOWLEDGMENTS

The authors thank Professor Benxun Su for providing the Luobusha and Stillwater spinel samples. We are also grateful to Professor Heidi Höfer and two anonymous reviewers for their critical reviews and Anneliese Lust and Wei Yang for the editorial work. This study was financially supported by the National Natural Science Foundation of China (41822202, 42002096), pre-research project on Civil Aerospace Technologies of China National Space Administration (D020203), and the Experimental Technology Innovation Fund of the Institute of Geology and Geophysics, Chinese Academy of Sciences (11990860).

REFERENCES

1. T. N. Irvine, *Can. J. Earth Sci.*, 1965, **4**, 71–103. https://doi.org/10.1139/e67-004
2. H. J. B. Dick and T. Bullen, *Contrib. Mineral. Petrol.*, 1984, **86**, 54–76. https://doi.org/10.1007/BF00373711
3. S. J. Barnes and P. L. Roeder, *J. Petrol.*, 2001, **42**, 2279–2302. https://doi.org/10.1093/petrology/42.12.2279
4. S. Arai and N. Akizawa, *Am. Mineral.*, 2014, **99**, 28–34. http://dx.doi.org/10.2138/am.2014.4473
5. V. S. Kamenetsky, A. J. Crawford, and S. Meffre, *J. Petrol.*, 2001, **42**, 655–671. https://doi.org/10.1093/petrology/42.4.655
6. S. Arai, *Chem. Geol.*, 1994, **113**, 191–204. https://doi.org/10.1016/0009-2541(94)90066-3
7. A. H. Ahmed, H. M. Helmy, S. Arai, and M. Yoshikawa, *Lithos*, 2008, **104**, 85–98. https://doi.org/10.1016/j.lithos.2007.11.009
8. M. F. Zhou, P. Robinson, B. X. Su, J. F. Gao, J. W. Li, J. S. Yang, and J. Malpas, *Gond. Res.*, 2014, **26**, 262–283. https://doi.org/10.1016/j.gr.2013.12.011
9. I. Uysal, A. Kapsiotis, R. M. Akmaz, S. Saka, and H. M. Seitz, *Ore Geol. Rev.*, 2018, **93**, 98–113. https://doi.org/10.1016/j.oregeorev.2017.12.017
10. C. Chen, B. X. Su, Y. Xiao, P. A. Sakyi, X. Q. He, K. N. Pang, I. Uysal, E. Avci, and L. P. Qin, *Lithos*, 2019, **342–343**, 361–369. https://doi.org/10.1016/j.lithos.2019.05.038
11. L. T. Bryndzia and B. J. Wood, *Am. J. Sci.*, 1990, **290**, 1093–1116. https://doi.org/ 10.2475/ajs.290.10.1093
12. C. Ballhaus, R. F. Berry, and D. H. Green, *Contrib. Mineral. Petrol.*, 1991, **107**, 27–40. https://doi.org/10.1007/BF00310615
13. C. Dupuis and G. Beaudoin, *Miner. Deposita*, 2011, **46**, 319–335. https://doi.org/10.1007/s00126-011-0334-y
14. S. A. S. Dare, S. J. Barnes, G. Beaudoin, J. Meric, E. Boutroy, and C. Potvin-Doucet, *Miner. Deposita*, 2014, **49**, 785–796. https://doi.org/10.1007/s00126-014-0529-0
15. H. G. E. Dien, S. Arai, L. S. Doucet, Z. X. Li, Y. Kil, D. Fougerouse, S. M. Reddy, D. W. Saxey, and M. Hamdy, *Nat. Comun.*, 2019, **10**, 5103. https://doi.org/10.1038/s41467-019-13117-1
16. X. Y. Song, K. Y. Wang, S. J. Barnes, J. N. Yi, L. M. Chen, and L. E. Schoneveld, *Am. Mineral.*, 2020, **105**, 479–497. https://doi.org/10.2138/am-2020-7222
17. W. Yang and Y. T. Lin, *The Innovation*, 2021, **2**, 100070. https://doi.org/10.1016/j.xinn.2020.100070
18. D. H. Lindsley, *Reviews in Mineralogy*, 1991, **25**, 509. https://doi.org/10.1016/0037-0738(93)90062-A
19. K. Righter, S. R. Sutton, M. Newville, L. Le, C. S. Schwandt, H. Uchida, and R. T. Downs, *Am. Mineral.*, 2006, **91**, 1643–1656. https://doi.org/10.2138/am.2006.2111
20. N. Ishizawa, K. Tateishi, S. Oishi, and S. Kishimoto, *Am. Mineral.*, 2014, **99**, 1528–1536. https://doi.org/10.2138/am.2014.4840
21. J. J. Papike, P. V. Burger, A. S. Bell, C. K. Shearer, L. Le, and J. Jones, *Am. Mineral.*, 2015, **100**, 2018–2025. https://doi.org/10.2138/am-2015-5208
22. J. Gross and A. H. Treiman, *J. Geophys. Res.*, 2011, **116**, E10009.

https://doi.org/10.1029/2011JE003858

23. T. C. Prissel, S. W. Parman, C. R. M. Jackson, M. J. Rutherford, P. C. Hess, J. W. Head, L. Cheek, D. Dhingra, and C. M. Pieters, *Earth Planet. Sci. Lett.*, 2014, **403**, 144–156. https://doi.org/10.1016/j.epsl.2014.06.027
24. T. C. Prissel, S. W. Parman, and J. W. Head, *Am. Mineral.*, 2016, **101**, 1624-1635. https://doi.org/10.2138/am-2016-5581
25. V. Colas, J. A. Padron-Navarta, J. M. Gonzalez-Jimenez, W. L. Griffin, I. Fanlo, S. Y. O'Reilly, F. Gervilla, J. A. Proenza, N. J. Pearson, and M. P. Escayola, *Am. Mineral.*, 2016, **101**, 1360–1372. https://doi.org/10.2138/am-2016-5611
26. S. E. Haggerty, *Am. Mineral.*, 2016, **101**, 5–6. http://doi.org/10.2138/am-2016-5554
27. Y. Bai, B. X. Su, Y. Xiao, D. Lenaz, P. A. Sakyi, Z. Liang, C. Chen, and S. H. Yang, *Minerals*, 2018, **8**, 62. https://doi.org/10.3390/min8020062
28. G. Ceuleneer, *Nature*, 2004, **432**, 156–157. https://doi.org/10.1038/432156a
29. C. A. McCammon, V. Chaskar, and G. G. Richards, *Meas. Sci. Technol.*, 1991, **2**, 657–662. https://doi.org/10.1088/0957-0233/2/7/014
30. B. J. Wood and D. Virgo, *Geochim. Cosmochim. Acta.*, 1989, **53**, 1277–1291. https://doi.org/10.1016/0016-7037(89)90062-8
31. D. O. Canil and H. S. C. Neill, *J. Petrol.*, 1996, **37**, 609–635. https://doi.org/10.1093/petrology/37.3.609
32. L. Galoisy, G. Calas, and M. A. Arrio, *Chem. Geol*, 2001, **174**, 307–319. https://doi.org/10.1016/S0009-2541(00)00322-3
33. M. Wilke, H. Behrens, D. J. M. Burkhard, and S. Rossano, *Chem. Geol.*, 2002, **189**, 55–67. https://doi.org/10.1016/S0009-2541(02)00042-6
34. A. J. Berry, H. S. C. O'Neill, K. D. Jayasuriya, S. J. Campbell, and G. J. Foran, *Am. Mineral.*, 2003, **88**, 967–977. https://doi.org/10.2138/am-2003-0704
35. P. A. van Aken, B. Liebscher, and V. J. Styrsa, *Phys. Chem. Miner.*, 1998, **25**, 323–327. https://doi.org/10.1007/s002690050122
36. L. A. J. Garvie and P. R. Buseck, *Nature*, 1998, 396, 667–670. https://doi.org/10.1038/25334
37. V. G. Batanova, J. M. Thompson, L. V. Danyushevsky, M. V. Portnyagin, D. Garbe-Schonberg, E. Hauri, J. I. Kimura, Q. Chang, R. Senda, K. Goemann, C. Chauvel, S. Campillo, D. A. Lonov, and A. V. Sobolev, *Geostand. Geoanal. Res.*, 2019, **43**, 453–473. https://doi.org/10.1111/ggr.12266
38. B. Su, Y. Chen, Q. Mao, D. Zhang, L. H. Jia, and S. Guo, *Lithos*, 2019, **344**–**345**, 207–216. https://doi.org/10.1016/j.lithos.2019.06.029
39. M. J. Pankhurst, R. Walshaw, and D. Morgan, *Geostand. Geoanal. Res.*, 2017, **41**, 85–91. https://doi.org/10.1111/ggr.12134
40. M. Fialin, A. Bezos, C. Wagner, V. Magnien, and E. Humler, *Am. Mineral.*, 2004, **89**, 654–662. https://doi.org/10.2138/am-2004-0421
41. H. E. Höfer and G. P. Brey, *Am. Mineral.*, 2007, **92**, 873–885. https://doi.org/10.2138/am.2007.2390
42. I. S. McCallum, *Dev. Petrol*, 1996, **15**, 441–483. https://doi.org/10.1016/S0167-2894(96)80015-7
43. T. C. Labotka and R. L. Kath, *Geol. Soc. Am. Bull.*, 2001, **113**, 1312–1323. https://doi.org/10.1130/0016-7606(2001)113<1312:POTCMR>2.0.CO;2
44. D. S. Xue, B. X. Su, D. P. Zhang, Y. H. Liu, J. J. Guo, Q. Guo, J. F. Sun, and S.Y. Zhang, *J. Anal. At. Spec.*, 2020. https://doi.org/doi:10.1039/D0JA00273A.
45. D. P. Zhang, D. S. Xue, Y. H. Liu, B. Wan, Q. Guo, and J. J. Guo, *Sensors*, 2020, **18**, 5325. https://doi.org/10.3390/s20185325
46. J. T. Armstrong, *Microbeam Analysis*, 1995, **4**, 177–200. https://www.mendeley.com/catalogue/9f24cb59-de6b-3c8c-aed9-5861cc3aad42/
47. S. T. Wu, G.Wörner, K. P. Jochum, B. Stoll, K. Simon, and A. Kronz, *Geostand. Geoanal. Res.*, 2019, **43**, 567–584. https://doi.org/10.1111/ggr.12301
48. W. Griffin, W. Powell, N. J. Pearson, and S. O'Reilly, *Mineralogical Association of Canada*, 2008, 308–311.
49. L. W. Xie,Y.B. Zhang, H. H. Zhang, J. F. Sun, and F. Y. Wu, *Chin. Sci. Bull.*, 2008, **53**, 1565–1573. https://doi.org/10.1007/s11434-008-0086-y
50. S. T. Wu, V. Karius, B. C. Schmidt, K. Simon, and G. Woerner, *Geostand. Geoanal. Res.*, 2018, **42**, 575–591. https://doi.org/10.1111/ggr.12230
51. M. D. Dyar, A. V. McGuire, and R. D. Ziegler, *Am. Mineral.*, 1989. **74**, 969–980. http://pubs.geoscienceworld.org/msa/ammin/article-pdf/74/9-10/969/4222103/am74_969.pdf
52. J. W. Delano, *Lunar Planet. Sci.*,1996, 303-304.
53. C. Zhang, R. R. Almeev, E. C. Hughes, A. A. Borisov, E. P. Wolff, H. E. Höfer, R. E. Botcharnikov, and J. Koepke, *Am. Mineral.*, 2018, **103**, 1445–1454. https://doi.org/10.2138/am-2018-6437
54. S. B. J. Reed, *Cambridge: Cambridge University Press*, 2005. https://doi.org/10.1017/CBO9780511610561
55. V. G. Batanova, A. V. Sobolev, and D. V. Kuzmin, *Chem. Geol.*, 2015, **419**, 149–157. https://doi.org/10.1016/j.chemgeo.2015.10.042
56. J. J. Donovan, H. A. Lowers, and B. G. Rusk, *Am. Mineral.*, 2011, **96**, 274–282. https://doi.org/10.2138/am.2011.3631
57. P. J. Potts, A. G. Tindle, and M. C. Isaacs, *Am. Mineral.*, 1983, **68**, 1237–1242. https://doi.org/10.1016/0040-1951(84)90122-7
58. K. P. Jochum, D. B. Dingwell, A. Rocholl, B. Stoll, A. W. Hofmann, S. Becher, A. Besmehn, D. Bessette, H. J. Dietze, P. Dulski, J. Erzinger, E. Hellebrand, P. Hoppe, I. Hom, K. Janssens, G. A. Jenner, M. Klein, W. F. McDonough, M. Maetz, K. Mezger, C. Munker, I. K. Nikogosian, C. Pickhardt, I. Raczek, D. Rhede, H. M. Seufert, S. G. Simakin, A. V. Sobolev, B. Spattel, S. Straub, L. Vincze, A. Wallianos, G. Wechwerth, S. Weyer, D. Wolf, and M. Zimmer, *Geostandard. Newslett.*, 2000, 24, 87–133. https://doi.org/10.1111/j.1751-908X.2000.tb00590.x
59. D. Harries, *Chem. Erde.*, 2014, **74**, 375–384. https://doi.org/10.1016/j.chemer.2014.01.001
60. F. A. Davis, E. Cottrell, S. K. Birner, J. M. Warren, and O. G. Lopez, *Am. Mineral.*, 2017, **102**, 421–435. https://doi.org/10.2138/am-2017-5823
61. J. F. Luhr and J. J. Aranda-Gómez, *J. Petrol.*, 1997, **38**, 1075–1112. https://doi.org/10.1093/petroj/38.8.1075